Climate Signals in River Flood Damages Emerge under Sound Regional Disaggregation

Inga Sauer
Potsdam Institute for Climate Impact Research, Telegraphenberg A 56, 14473 Potsdam, Germany
https://orcid.org/0000-0002-9302-2131

Ronja Reese
Potsdam Institute for Climate Impact Research, Telegraphenberg A 56, 14473 Potsdam, Germany
https://orcid.org/0000-0001-7625-040X

Christian Otto
Potsdam Institute for Climate Impact Research, Telegraphenberg A 56, 14473 Potsdam, Germany
https://orcid.org/0000-0001-5500-6774

Tobias Geiger
Potsdam Institute for Climate Impact Research, Telegraphenberg A 56, 14473 Potsdam, Germany

Sven N. Willner
Potsdam Institute for Climate Impact Research, Telegraphenberg A 56, 14473 Potsdam, Germany
https://orcid.org/0000-0001-6798-6247

Benoit Guillod
Institute for Environmental Decisions, ETH Zurich, Universitätstr. 22, 8092 Zurich, Switzerland
https://orcid.org/0000-0003-1807-6997

David Bresch
Institute for Environmental Decisions, ETH Zurich, Universitätstr. 22, 8092 Zurich, Switzerland
https://orcid.org/0000-0002-8431-4263

Katja Frieler (katja.frieler@pik-potsdam.de)
Potsdam Institute for Climate Impact Research, Telegraphenberg A 56, 14473 Potsdam, Germany
https://orcid.org/0000-0003-4869-3013

Article

Keywords: precipitation patterns, climate change, fluvial flood, fluvial, hydrological simulation, damages, climate signal

Posted Date: June 30th, 2020

DOI: https://doi.org/10.21203/rs.3.rs-37259/v1

Version of Record: A version of this preprint was published at Nature Communications on April 9th, 2021.
See the published version at https://doi.org/10.1038/s41467-021-22153-9.

Climate signals in river flood damages emerge under sound regional disaggregation

Inga Sauer[1,2], Ronja Reese[1], Christian Otto[1], Tobias Geiger[1,3], Sven N. Willner[1], Benoit Guillod[2,4*], David N. Bresch[2,5] , and Katja Frieler[1]

1 Potsdam Institute for Climate Impact Research, Telegraphenberg A 56, 14473 Potsdam, Germany
2 Institute for Environmental Decisions, ETH Zurich, Universitätstr. 22, 8092 Zurich, Switzerland
3 German Meteorological Service (DWD), Climate and Environment Consultancy, Güterfelder Damm 87-91, 14532 Stahnsdorf, Germany
4 Institute for Atmospheric and Climate Science, ETH Zurich, Universitätstr. 22, 8092 Zurich, Switzerland
* current affiliation: CelsiusPro AG, Seebahnstrasse 85, 8003 Zürich, Switzerland
5 Federal Office of Meteorology and Climatology MeteoSwiss, Operation Center 1, P.O. Box 257, 8058 Zurich-Airport, Switzerland

Abstract

Climate change highly affects precipitation patterns. Here, we address the question whether the signal of climate change is already detectable in time series of reported damages caused by fluvial floods. Building on hazard indicators from process-based hydrological simulations, we develop an empirical model to reconstruct reported damages and quantify individual contributions of climate-induced changes in hazard, exposure, and vulnerability to observed trends. Across nine world regions, trends in damages are generally dominated by increasing exposure and decreasing vulnerability, with the latter being most pronounced in less developed regions. However, accounting for heterogeneity in changes of hazard frequency and magnitude within a region, a climate signal is detectable, especially in South and Sub-Saharan Africa as well as in Latin America. Damages in most regions are subject to a monotonous trend even after accounting for natural variability where an effect of long-term global warming can not yet be distinguished from a potential influence from multidecadal oscillations.

Main

Since 1980, fluvial floods have caused more than 200,000 fatalities and more than $790 bn in direct economic damages, globally[1], placing them among the most socially and economically devastating natural disasters. Theoretical considerations on the global surface energy budget suggest that global mean precipitation increases with global mean temperature (GMT) at a rate of 1-2% per K[2]. However, most relevant for fluvial flood risk extreme precipitation events are[3] and their intensity increases with the moisture of air that can be precipitated out according to the Clausius-Clapeyron relationship[4], and therefore extreme daily precipitation is expected to scale at a substantially higher rate of ~6-7% per K[5]. These theoretical considerations were recently confirmed by observations showing a global median increase in annual maximum daily precipitation of 5.9% to 7.7% per degree of global warming[6] and more record-breaking rainfall events than expected in a stationary climate (12% increase in 1981–2010[7]). Further,

the observed intensification of extreme daily precipitation events since the 1980ies have been recently attributed to anthropogenic global warming[8]. Observed annual discharge maxima show regionally varying trends with significant increases in most stations of Asia, Europe and Latin America and mostly decreasing trends in Africa, Australia and North America[9]. Globally, 1985-2009 flood frequency has first increased, peaked around 2003, and eventually decreased afterwards [10]. Extreme flood events show a similar non-monotonous temporal evolution with strongest long term trends in Europe and the United States of America[11]. On global and latitudinal scales the observed variation in flood frequencies can be statistically explained by variations of four decadal and multi-decadal climate oscillations: the El Niño–Southern Oscillation (ENSO), the Pacific Decadal Oscillation (PDO), the North Atlantic Oscillation (NAO), and the Atlantic Multidecadal Oscillation (AMO)[10]. Here, we focus on economic damages caused by fluvial flooding and investigate to what extent climate change has already induced long-term trends. To disentangle the impact of climate induced changes in weather-related hazards (flood extent and depth) from changes in exposure of assets, and their vulnerability, we develop a semi-empirical model where annual flooded areas are derived from hydrological simulations forced by observational weather data[12, 13], overlaid with spatially and temporally explicit asset distributions. Derived exposed assets are translated into direct economic damages by damage functions[14] allowing for time dependent vulnerability factors[12, 13, 15] (Methods and supplementary Figs. SI1, SI2). Globally, trends in flood-induced damages have been shown to be dominated by increasing exposure and decreasing vulnerability[12, 13, 15], i.e., no detectable potentially climate-driven trend remains after removal of socio-economic effects at the global scale as well as on the level of world regions. This finding is irrespective of the regions' development level [12, 16, 17, 18] and income groups[12]. However, these studies focus on the detection of changes in vulnerability and therefore considered world regions that have been defined to be homogeneous with respect to socio-economic indicators, but not with regard to climate-induced changes in weather-related hazard indicators. This aggregation across heterogeneous trends in hazards could hide the signal of climate change. To avoid this, we first verify that discharge trends modeled by global hydrological models (GHMs) (Fig. 1a) compare well with observed trends [9, 19, 20, 21], when the GHMs are driven by observed weather data (Methods and Supplementary Information (SI) Sec. 4). We then use the modeled trends to divide 9 standard, socio-economically homogeneous world regions (R)[22] into subregions R_+ and R_- with positive and negative trends in discharge, respectively (Fig. 1b and Methods).

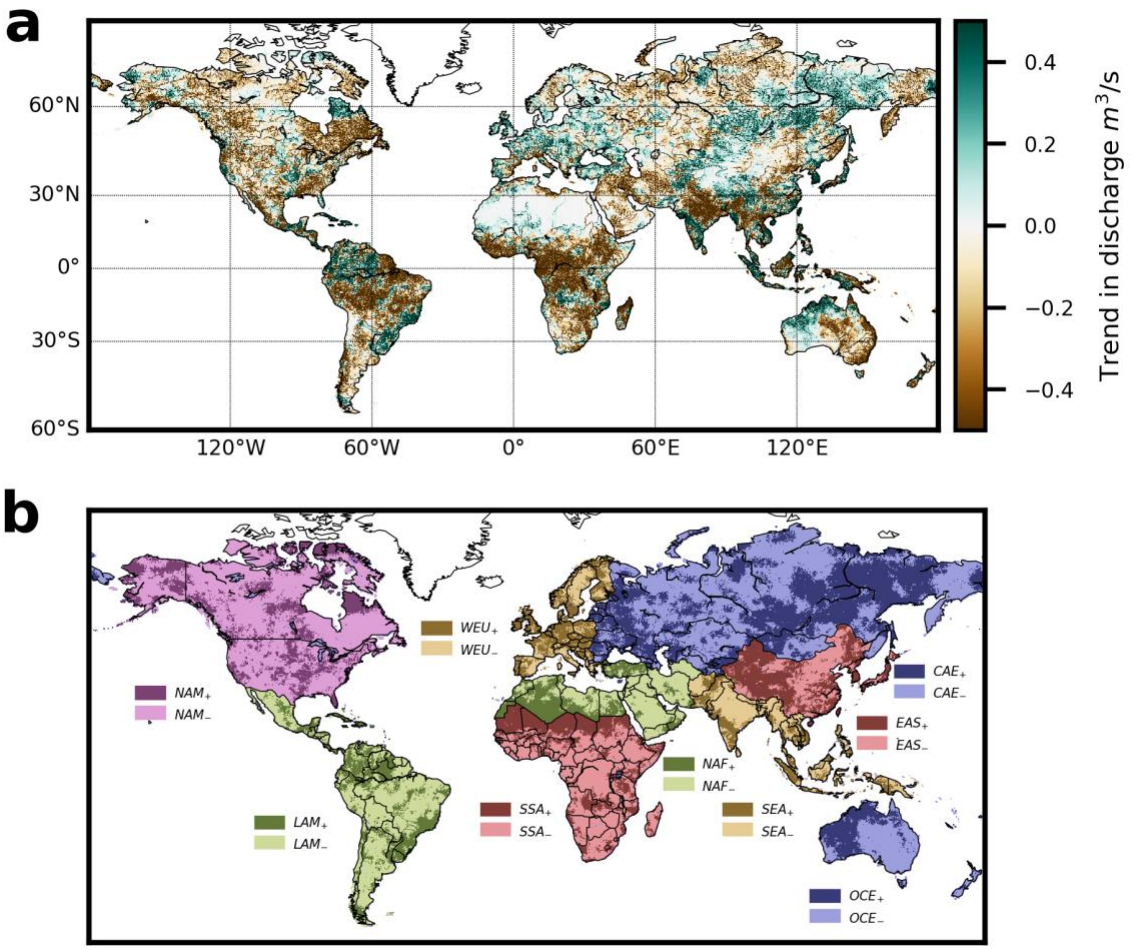

Figure 1: Discharge trends and definition of regions. a *Absolute trends in annual maximum discharge in the time period 1971-2010 (significance levels are shown in supplementary Fig. SI3)* **b** *Map of the nine geographical world regions: North America (NAM), Eastern Asia (EAS), Western Europe (WEU), Latin America (LAM), Central Asia & Eastern Europe (CAE), South & Sub-Saharan Africa (SSA), South & South-East Asia (SEA), North Africa & Middle East (NAF), Oceania (OCE) chosen according to geographical proximity and similarity of socio-economic structure. These regions are then further divided into subregions with positive (R_+, dark colors) and negative discharge trends (R_-, light colors).*

Climate signal in flood damages. When analyzing the contributions of the individual drivers to damage trends, we focus on regions where the full model accounting for all three drivers) explains at least 30% of the variance in reported damages (gray panels in Fig. 2) indicating that at least part of the critical processes determining the variability in damages are captured. In North America (NAM), the explanatory power is exceptionally high (R^2_{NAM}> 90%, R^2_{NAM+}>70%, R^2_{NAM-} > 95%), but reaches also more than 60% in Eastern Asia (EAS) (~40% in its subregions) and in subregions of Latin America (LAM) and Oceania (OCE). In Western Europe (WEU) and South & Sub-Saharan Africa (SSA), the explanatory power is also good (R^2> 30%). Unexplained variations may be rooted in unsystematic reporting errors or biases in damages[23], varying performance of GHMs across hydrobelts[24] , limited quality of the forcing data sets[25], and depth-damage functions (Methods).

Climate-induced trends in damages are estimated from a restricted model accounting only for observed daily weather fluctuations while keeping exposure (in units of inflation adjusted 2005 purchasing power parities (PPP) USD) and vulnerability at 1980 levels ($D_{Cli\text{-}1980}$). Damage trends induced by changes in exposure are then estimated from the difference between the trend in $D_{Cli\text{-}1980}$ and the trend derived from an extended model additionally accounting for changes in exposure (D_{CliExp}). Finally, damage trends induced by changes in vulnerability are estimated from the difference in trends between D_{CliExp} and the full model (D_{Full}) (Methods). In line with previous studies[12, 13, 15, 26], we find that trends in total damages mainly result from an increase in exposure that is moderated by a reduction in vulnerability (Fig. 2). This general picture is particularly visible in LAM (and its subregions), in EAS, in South & South Eastern Asia (SEA), and in North Africa & Middle East (NAF). Exposure trends are exclusively positive and mostly significant, except in OCE. We find mostly decreasing vulnerability levels with the exception of Western Europe and North America, where vulnerability has increased. In LAM a strong reduction in vulnerability has widely overcompensated increasing exposure and led to an overall reduction in damages, also in the subregion with decreasing discharge trends LAM_-. By contrast, in LAM_+, the increase in both, climate induced trends and trends in exposure, has led to a positive trend in modeled damages that is perfectly in line with the observed trend and not compensated by the vulnerability reduction. With the exception of SSA, weather-induced trends in the regions are small compared to exposure and vulnerability-induced trends and mostly insignificant. However, when splitting up the world regions into their subregions with homogeneous discharge trends, climate-induced trends become clearly detectable (Fig. 2). The climate contribution is strongest in SSA_+, where it exceeds the socio-economic contributions by far. Indeed, we find the positive significant damage trend in this subregion can be majorly attributed to climatic effects. In several subregions that have become wetter (SEA_+, NAF_+, and especially OCE_+), the climate-induced trends are comparable or even larger than the trends induced by the socio-economic drivers. Though, we have to caution that the explanatory power of our model is low in these subregions ($R^2 < 30\%$). In subregions with negative climate-induced trends, the climate signal translates into negative contributions to damage trends (e.g. OCE_-), but it is not strong enough to lead to an overall reduction in damages, except in LAM_- and SSA_-. However, in these two regions the decline is not in line with observations.

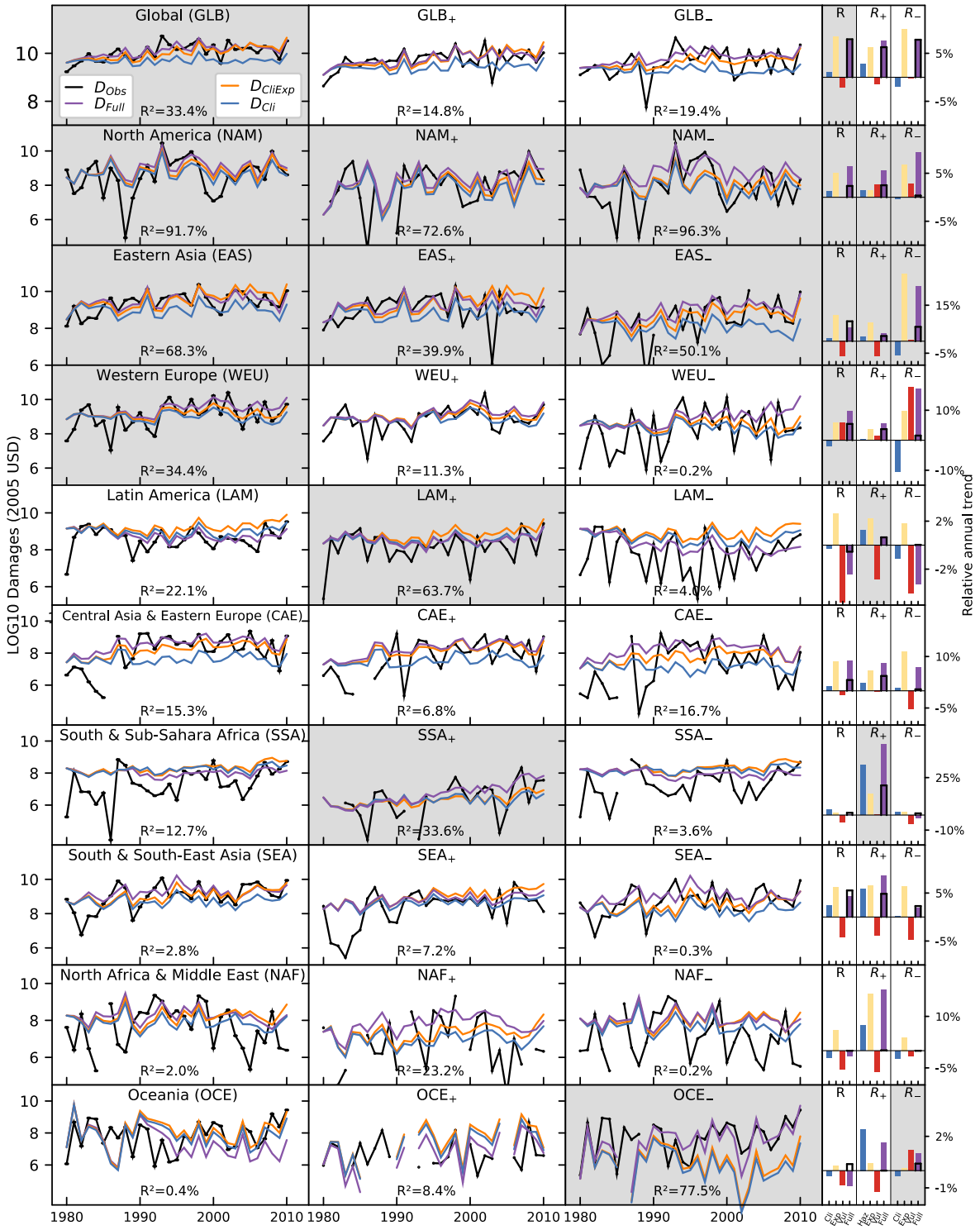

Figure 2: Contributions of changes in climate, exposure, and vulnerability to damages induced by river floods (1980-2010): *Time series of observed damages (NatCatService database[1] (black) as well as modeled damages (multi-model median) when accounting for changes in i) climate only (constant 1980 socio-economic conditions, $D_{Cli\text{-}1980}$, blue), ii) climate and exposure (D_{CliExp}, orange) keeping vulnerability at 1980 conditions, and iii) in climate, exposure, and vulnerability (D_{Full}, purple) over time for the nine world regions (left main panel), as well as their subregions with homogeneous positive and negative trends in river discharge (middle and right main panels) (cf. Fig. 1). Left Bars in the side panel on the right indicate the*

relative trend in annual modeled (Full, purple) and observed damages (Full, black squares) and the individual contributions of each driver: climate variability (Cli, blue), exposure (Exp, yellow), vulnerability (Vul, red). R^2 indicates the explained variance of the full model compared to the observed damages. Time series indicating the model-spread are provided in supplementary Fig. SI4.

While the damage reporting by Munich Re's NatCatSERVICE only starts in 1980, the ISIMIP2a hydrological simulations start nine years earlier in 1971 allowing for a backward extension of simulated damages. The trends in damages are generally robust with respect to the backwards extension, except for OCE and WEU (Fig. 3). In several regions, climate induced trends become significant and clearly show the relevance of the considered subregions when determining the detectability of climate change in flood damages. For instance, in most R_+regions, we find positive and significant climate-induced trends in simulated damages over the period 1971-2010, whereas these trends remain insignificant in most geographical regions, except for EAS and SSA. Climate-induced positive trends are most pronounced in SSA_+ ($Cli_{SSA+\,2010} = 19.1\,\%/year$) (exact numbers for all regions are given in supplementary Tab. SI2). The positive trend in $SSA_$demonstrates that trends in annual maximum discharge do not necessarily translate into similar trends in damages as the translation of discharge into damages is asymmetric: high discharge levels may lead to economic damages when protection standards are exceeded, while low discharge levels influence discharge trends but are irrelevant for flood damages.

To check the robustness of the climate-induced trends with regard to the choice of the baseline year for the socioeconomic forcing, we additionally calculate the damage time series and derive climate-induced trends (Cli_{2010}) for fixed 2010 socio-economic conditions, which does not significantly alter the climate induced-trends (Fig. 3 and supplementary Fig. SI5). The (Cli_{2010}) trend also allows to quantify the contribution of climate from 1980-2010 (or 1971 - 2010) to median damages in 2010 as difference between the start level of the regression line and its end level (supplementary Tab. SI2).

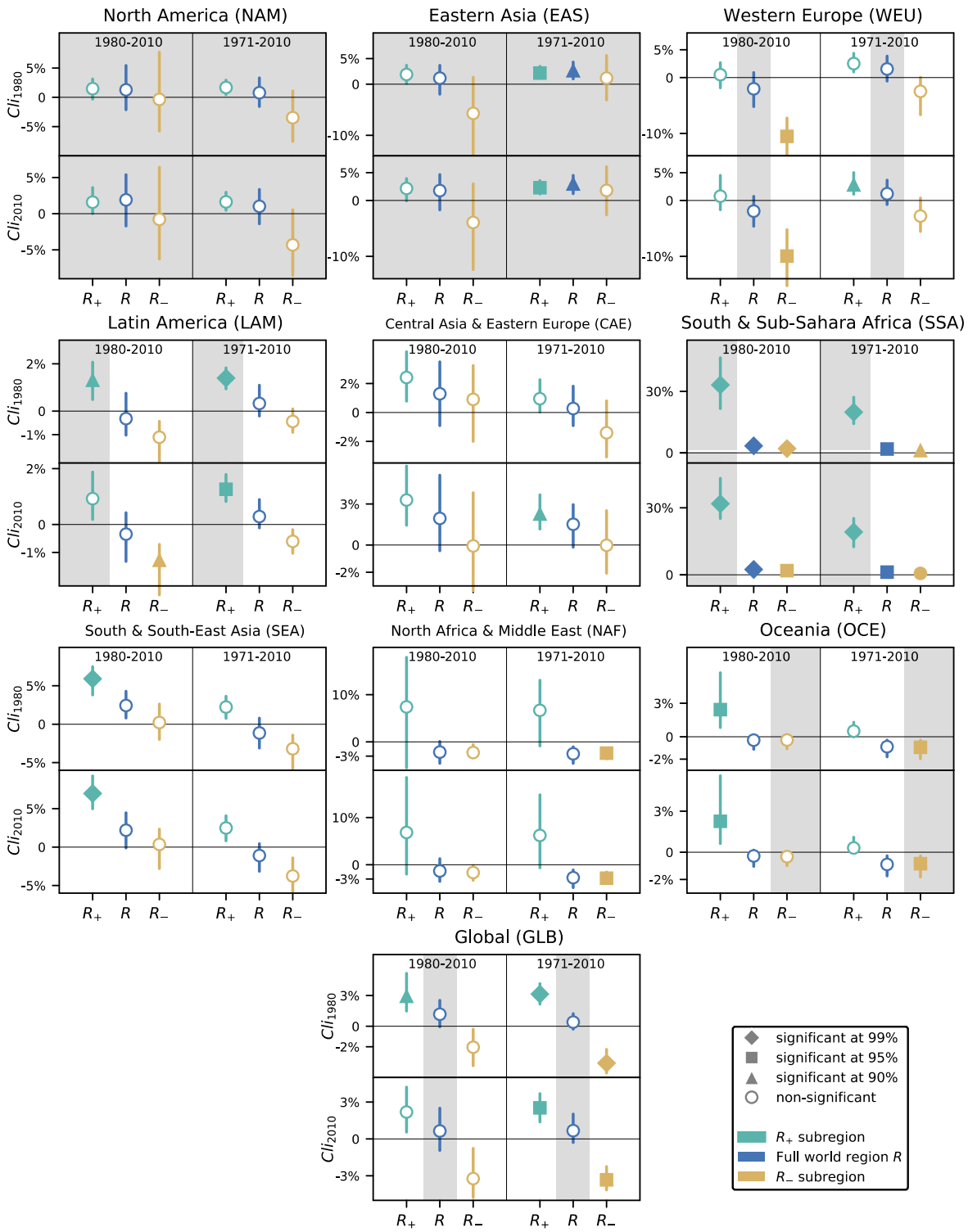

Figure 3: Climate induced trends in economic damages. *Shown are trends for each geographical world region (R, blue) as well as in the subregions with positive (R_+, turquoise bars) and negative discharge trends (R_-, brown bars). Uncertainty bars mark the ⅓ and the ⅔ quantile of the Theil-Sen-slope estimation. Symbols indicate the statistical significance of the climate trends at various levels. Grey shadings indicate subregions with high explained*

variance (R^2 > 30%). Climate-induced trends are calculated for fixed 1980 exposure (Cli_{1980}) and fixed 2010 exposure (Cli_{2010}).

Drivers of climate induced damage trends. To assess whether climate-induced trends in damages will persist in the future due to ongoing anthropogenic climate change or whether they are temporary and caused by climate oscillations (which would make them highly sensitive to the considered time period), we test to what degree the modeled time series of climate-induced damages for the full period 1971-2010 ($D_{Cli\text{-}1980}$) can be explained by variations in ENSO, PDO, NAO, AMO and GMT. The latter is considered a proxy for long-term monotonous climate change[27]. In the given time period from 1971-2010, the AMO index is highly correlated with GMT (Pearson correlation coefficient r = 0.92) and shows a similar monotonous increase (Fig. 4a) such that it can be considered a replacement of GMT in many cases. Therefore, we identify the model providing the best representation of the simulated damages while avoiding overfitting based on a "leave-one-out-cross-validation" (LooCV)[28] for two separate trend analyses; in the first, the best predictors are chosen among ENSO, PDO, NAO, and GMT, and (Fig. 4b), in the second, the best predictors are chosen among all four climate oscillations (replacing GMT by AMO) (Fig. 4c) (Methods). From all regions where the explained variance of the full model (D_{Full}) is high (R^2> 30%) (GLB, NAM_+, NAM, NAM_-, EAS_+, EAS, EAS_-, WEU, LAM_+, SSA_+,and OCE_-), either GMT or AMO are significant predictors for the monotonous long-term trend in climate induced damages (Fig. 4c). The explanatory power of the best models are similar, regardless whether AMO or GMT are contained in the set of predictors (Table SI4). It has been argued that the observed AMO should be viewed as a combination of both, internal variability and responses to external forcings[29, 30, 31] and does not permit to rule out the effect of anthropogenic forcing even when AMO is the best predictor. Thus, while we cannot distinguish between the effects of GMT and AMO, our analysis should be considered as a test for a potential long-term monotonous trend given large scale climate oscillations. Future availability of longer time series, e.g., extending the data up to 2020, may allow us to disentangle the effects of AMO and GMT more robustly.

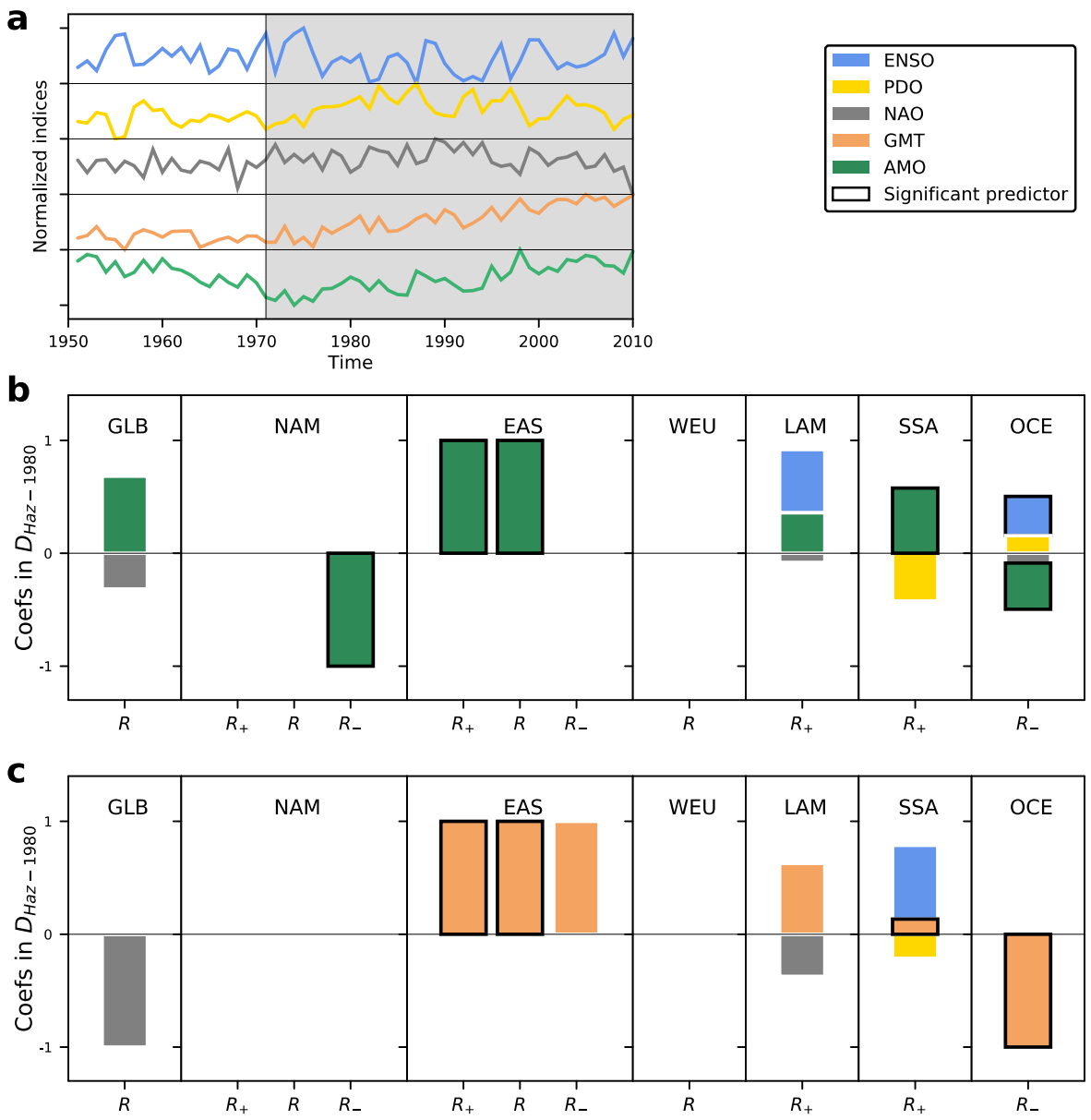

Figure 4: Predictors of climate-induced trends in flood damages. ***a*** *Normalized indices of ENSO, PDO, NAO, AMO, and GMT from 1971-2010. Only the period 1971-2010 is used for the analysis (gray shading).* ***b*** *Relative shares of the coefficients (Methods) of the linear predictors (ENSO, PDO, NAO, and AMO) included in the best model (according to the leave-one-out-Cross-Validation) for the damage time series accounting for climate induced trends only (fixed 1980 exposure and vulnerability). Shown are only regions with* $R_2 > 30\%$ *for the full model of Fig. 1. Black boxes indicate significant predictors at 90% level.* ***c*** *Same as* ***b****, but using ENSO, PDO, NAO, and GMT as predictors.*

Discussion. In many regions, the quantification of the contribution of climate change to observed trends in flood induced economic damages is still limited by an insufficient understanding of the observed damage time series. First of all, coarse and uncalibrated hydrological simulations such as those used here may not be able to properly reproduce the interannual variability of observed damages. In addition, due to the use of multi-model

medians of damage time series, modeled time series are assumed to have a relatively smaller variability than the recorded damages, explaining the differences in the significance levels between observed and modeled damage trends. However, the excellent reproduction of observed fluctuations in damages in North America underlines the explanatory power of the considered modelling approach. The general performance of the hydrological models is also demonstrated by the close agreement between simulated and observed trends in discharge [9, 19, 20, 21] (SI Sec. 4). Especially, for large-scale climate change impact assessments, as the trend analysis undertaken here, they have been found to be a suitable tool [32]. Qualitatively, observed and modeled damage trends match in all world regions and subregions, except for OCE, $SSA\_$, $NAF\_$, $LAM\_$. Unexplained variances of observed damage data may result from regional deficits in reported damages, observational climate forcings, representation of protection standards, or asset distributions. Our analysis highlights the importance of subregional differences in impacts and the need for spatially-explicit and event-specific damage records to allow for a high-regional detail in the assignment of damages. The geo-codes provided in the NatCatSERVICE database are a good starting point in this regard, but more accurate event footprints are desirable for a better regional assignment of damages.

Here, we estimate vulnerability from the ratio of observed and simulated damages as obtained when accounting for climate and exposure driven changes in damages (D_{CliExp}). In consequence, misrepresentation of trends in either the reported, or simulated climate and exposure-driven damages will reflect in changes in vulnerability over time. For example, an underreporting of damages in early years would erroneously translate into low vulnerabilities in the early phase. Similarly, too low estimates of the climate-induced trends could be compensated by increasing vulnerability estimates. We find mostly decreasing vulnerability trends indicating that both effects may only play a limited role. Robust increases in vulnerability are only identified in Western Europe and North America (Fig. 3, supplementary Figs. SI1 and SI2), where the data quality of reported damages is assumed to be high. Increasing vulnerabilities in high developed regions may particularly occur due to behavioural changes caused by better assumed protection, e.g. the levee effect[33]. In addition, vulnerability is assumed to change slowly over time, while the good reproduction of annual fluctuations in reported damages may be an indicator for a high quality of the observational climate data and translation into flood hazards. In previous studies, mostly decreasing vulnerabilities with overall converging trends between high- and low-income countries have been found[12, 15]. However, also increasing vulnerability levels have been reported for higher-middle income countries [13]. Differences to our findings may be explained by the aggregation over countries by income and not with regard to geographical closeness or discharge trends and considerations of different time periods. Our quantification of climate change contributions to observed trends in flood-induced damages differs from “climate impacts attribution” as defined in chapter 18 of the IPCC AR5[34]: “Detection of impacts’ of climate change addresses the question of whether a natural or human system is changing beyond a specified baseline that characterizes its behavior in the absence of climate change.”[35] where this “baseline may be stationary or non-stationary (e.g., due to land use change)”. According to this definition, the impacts of climate change on observed trends in flood-induced damages would have to be estimated as the difference between observations and damages derived from simulation assuming stationary climate and observed changes in asset distributions and vulnerabilities. In contrast, we estimate them from a varying climate but with fixed asset distributions and vulnerabilities. However, the contributions of climate change to average damages at the end of the considered time period (2010) - estimated by multiplying climate induced trends (1980-

2010) assuming fixed 2010 socio-economic conditions with the length of the time period - basically corresponds to the AR5 definition of impact attribution in 2010. As such, our approach certainly only quantifies the contribution of climate change over the 1980-2010 period and not the full contribution of climate change compared to pre-industrial levels.

Conclusions. It is critical to identify the individual drivers of flood-induced damages since their mitigation may require different mitigation and coping strategies. We demonstrate that averaging across regions with heterogeneous climate induced trends in flood hazards can hide the signal of climate change in reported time series of flood-induced damages. While previous global studies suggest that the contributions of climate to changes in flood damages have been minor compared to socio-economic drivers, we show that the impacts of climate change become detectable on subregional level, especially in regions of Sub-Saharan Africa, Eastern Asia, and Latin America. The considered "semi-empirical" modelling approach building upon process-based hydrological simulations and empirical estimates of vulnerabilities proves to be a powerful tool to attribute observed damages induced by river floods. While remote sensing may allow for the identification of flooded areas in recent years making use of the MODerate resolution Imaging Spectro-radiometer (MODIS) instruments on the NASA Aqua and Terra satellites[36], process-based modelling remains critical, both for backward extensions required for the attribution of long-term trends and for future climate impacts projections.

The generation of stationary counterfactual historical climate forcing data[37] and their translation into flooded areas based on hydrological simulations will also allow us to apply our framework to the attribution of observed impacts as defined by the AR5. Whereas, based on the ISIMIP2a simulations (1971-2010), it was not yet possible to decide whether the climate induced change in damages is attributable to long-term warming or natural climate variability, the inclusion of the recent decade may already enable us to provide a clearer answer. Nonetheless, our analysis clearly reveals an underlying monotonous climate-induced trend in damages in many regions that prevails over the trends induced by the climate oscillations ENSO, NAO, and PDO.

Methods

Trend estimation. Throughout this work, we use the Theil-Sen Slope estimator[38] to quantify trends and apply the non-parametric Mann-Kendall test[39] to evaluate significance levels. In the damage analyses, trends are relative to the annual mean damage of the reference period 1980-1990 in the corresponding region or subregion.

Flood modeling and definition of subregions by discharge trends. We subdivide the nine geographical world regions into subregions with positive and negative trends in annual discharge maxima over the period 1971-2010. Studies on changes in global discharge patterns are rare and data coverage is not evenly distributed around the globe. Furthermore, the susceptibility of discharge to human intervention affects discharge records and complicates disentangling human and climatic forces in observations. We therefore derive discharge trends from the harmonized multi-model simulations of the 12 global gridded hydrological models (GHM) participating in phase 2a of the Inter-Sectoral Impact Model Intercomparison Project (ISIMIP2a[40]). We here apply the naturalized experiment referred to as 'NOSOC' in the ISIMIP2a protocol, meaning that no human impacts, such as dams and

water abstractions on river flow were considered. This is legitimate for two reasons: 1) to ensure consistency with river routing simulations that do not account for human regulation of rivers, and 2) based on a previous study for some major basins that showed that the shape of the hydrograph, for peak daily flow, is not significantly different between natural and human impact experiments[41]. Furthermore, this allows us to better isolate climate induced changes in river discharge (SI Sec 3.1).

Here, the 12 GHMs were driven by four separate observational (atmospheric) weather data products for the period 1971-2010 providing daily runoff at 30arcmin resolution. For this ensemble of 46 climate data/GHM combinations (supplementary Tab. SI1), we follow the methodology applied previously in Willner et al. (2018a,b)[42, 43], and first harmonize the output of the different GHMs with respect to their fluvial network using the fluvial routing model CaMa-Flood (version 3.6.2[44]) yielding daily fluvial discharge at 15arcmin resolution. Especially for peak discharges, CaMa-Flood agrees better with observed fluvial discharges than the direct output of the hydrological models[45]. For the subsequent analysis, we then select the annual maximum daily discharge for each grid cell.

For each of the 46 simulations of daily fluvial discharge and each grid cell on 15arcmin resolution, we fit a generalized extreme value (GEV) distribution to the historical time series of the annual maximum discharge using L-moment estimators of the distribution parameters (for details see SI Sec 3.2 and discussion in Willner et al. (2018a)[42]) allowing for a model bias correction following the approach by [46]. It has been shown in several recent publications that such a hydrological modeling chain is able to reproduce patterns in observed flood impacts [12, 13]. In addition to these previous studies, we account for current flood protection standards at the sub-national scale from the FLOPROS database[47]. For the final assessment, we re-aggregate the high resolution flood depth data to a 2.5arcmin resolution by retaining the maximum flood depth as well as the flooded area fraction, defined as the fraction of all underlying high resolution grid cells where the flood depth was larger than zero.

Socio-economic data sources. We use gridded Gross Domestic Product (GDP) data reported in purchasing power parity (PPP) in 2005 USD from the ISIMIP project[48] with a spatial resolution of 5arcmin from 1971-2010 as a proxy for the distribution of assets. Gridded GDP data was obtained using a downscaling methodology [49] in combination with spatially-explicit population distributions from the History Database of the Global Environment (HYDE v3.2)[50, 51] and national GDP estimates[52]. Downscaled GDP data is available in 10y increments and linearly interpolated across decades. To estimate asset values more precisely we convert gridded GDP data into gridded capital stock, using annual national data on capital stock (in PPP 2005 USD) and GDP from the Penn World Table (version 9.1, https://www.rug.nl/ggdc/productivity/pwt/). For each country the annual ratio of national GDP and capital stock was calculated and smoothed with a 10-year running mean to generate a conversion factor, which was then applied to translate exposed GDP into asset values.

Observed asset damages are taken from reported flood damages from the NatCatSERVICE[1] database collected by MunichRe since 1980, excluding flash flood events or flooding caused by tropical cyclones. We adjusted all flood damage estimates for inflation to the reference year 2005 using country-specific consumer price indices (CPI), i.e., expressing them in the same base year as the GDP data. To do so, we constructed a conversion factor for each country based on all reported damages for a country-specific event in 2005 and the regularly CPI-

adjusted values reported in Munich Re's NatCatSERVICE database in the base year 2016. Multiplying CPI-adjusted reported flood damages by this conversion factor results in CPI-adjusted damages for 2005. Event-specific damage estimates were then aggregated to year-country and year-region level in order to be comparable with simulated river floods for which only the annual maximum was considered. Thereby we assumed that only one flood event is observed at each grid cell during a year. To resolve recorded damages in the refined subregional analysis, we make use of the geocodes given for each general flood event in the NatCatSERVICE dataset and assign the damage to the risk area of the centroid closest to the geocode location.

Economic damage assessment. For the estimation of direct asset damages, we apply the regional residential flood depth-damage functions developed by Huizinga et al. (2017) [14](SI Sec. 3.3). The quantification of flood damages consists of following steps: 1) determine exposed assets on the grid-level (150 arcmins resolution) based on the flooded fraction obtained from the inundation modelling; 2) determine the grid level damage by multiplying the exposed assets by the flood depth and the flood-depth damage function; 3) aggregate the estimated damages spatially to regional/subregional level, and 4) analyze the aggregated damages across different GHM simulations, assessing model medians and model spread. For steps 1 to 3, the open-source probabilistic natural catastrophe damage framework CLIMADA was used[53]. To account for the inhomogeneous but a priori unknown distribution of assets within a grid cell we additionally assume that no assets are exposed to a two-year flood event, thus subtracting the two-year flooded fractions from the modeled flooded fraction before multiplying with the asset value. This is equivalent to assuming that nobody would construct valuable assets in regions flooded every two years.

The modeled damages for each GHM and grid cell are then aggregated to country and region level. For comparability reasons we first aggregate to 9 world regions constructed by grouping countries with geographical proximity and similar socio-economic structure following the the income group classification of the Worldbank[22] (Fig. 1b). For regions and subregions, the median across all GHMs is then compared to reported damages from MunichRe's NatCatSERVICE (Fig 2).

Assessing and accounting for vulnerability. To include time-varying vulnerability, we apply an approach proposed in previous vulnerability studies[12, 13, 15]. Comparing modeled and observed damages, a time trend in the ratio of observed and modeled damages can be observed that can most likely be explained by changes in socio-economic vulnerability and/or adaptive capacity. These changes are not properly reflected within the modeling chain and are, e.g., caused by the fact that the protection standards underlying the FLOPROS database are stationary in time. We apply an 11-year smoothing on the ratio of reported and modeled damages using Singular Spectrum Analysis (SSA) (Fig. SI1 and Fig SI2)[54] assuming a maximum ratio of observed and modeled damages of 1000 to remove outliers. Before applying the SSA, missing values were replaced by the median ratio between 1980 and 2010.

Attributing damages to individual drivers. Given that the overall trend in damage time series is a superposition of the trends from each individual driver, we can separate the contributions from each driver by calculating the trend α of each time series $D_{Cli-1980}$, D_{CliExp}

and D_{Full} and extract climate induced trends in hazard, as well as trends in exposure and vulnerability, according to:

$$
\begin{aligned}
Cli_{R1980} &= \frac{\alpha_{Cli-R\,1980}}{n_R}, \\
Exp_R &= \frac{\alpha_{CliExp-R} - \alpha_{Cli-R1980}}{n_R}, \\
Vul_R &= \frac{\alpha_{Full-R} - \alpha_{CliExp-R}}{n_R},
\end{aligned}
\tag{1}
$$

We apply a non-parametric trend analysis (Theil-Sen Slope estimator) to estimate α. Trends are given relative to the annual reported average damages in the time period 1980-1990 (n_R) in each region or subregion (side panels in Fig. 2). We additionally provide climate induced trends from time series with 2010 fixed socio-economic conditions (Fig. 3):

$$Cli_{R2010} = \frac{\alpha_{Cli-R2010}}{n_R} \tag{2}$$

Socio-economic trends are assessed from 1980-2010. As climate induced trends are independent from observational data, we can extend it backward, making use of the full ISIMIP2a time period and additionally assess trends from 1971-2010.

Climate oscillations and global mean temperature. In order to avoid interferences with long term temperature increase, we use the pressure based Southern Oscillation Index as a predictor for ENSO (https://www.ncdc.noaa.gov/teleconnections/enso/enso-tech.php). Monthly data for AMO and NAO were extracted from the NOAA/Earth System Research Laboratory (https://www.psl.noaa.gov/data/climateindices/list/) and PDO from the NOAA/Climate Prediction Center (https://www.psl.noaa.gov/data/climateindices/list/). We derived annual GMT (daily mean Near-Surface Air Temperature) as the mean of three of the four input climate forcings provided in ISIMIP2a. We excluded the WATCH dataset because it does not capture the full historical period.

Contribution of global mean temperature and climate oscillations to climate induced damage trends. Following the methodology introduced by Najibi & Devineni (2018) and Armal et al. (2018), we apply generalized linear models (GLM) assuming damages to be log-normally distributed and assuming fixed 1980 socio-economic conditions (D_{Cli})[10, 27]. In a stepwise procedure we calculated GLMs from all possible combinations of the predictors ENSO, PDO, NAO, AMO, and GMT and a constant β:

$$D_{Cli} = \alpha_{ENSO} \cdot ENSO + \alpha_{PDO} \cdot PDO + \alpha_{NAO} \cdot NAO + \alpha_{GMT} \cdot GMT + \beta_2 \tag{3}$$

$$D_{Cli} = \alpha_{ENSO} \cdot ENSO + \alpha_{PDO} \cdot PDO + \alpha_{NAO} \cdot NAO + \alpha_{AMO} \cdot AMO + \beta_1 \tag{4}$$

We then select the best model applying a leave-one-out-Cross-Validation (LooCV) [28], which allows to assess model quality outside the fitting period calculating the “out-of-sample-error” (Supplementary Tab. SI4). The best model is the one with the smallest “out-of-sample-error”, we additionally test different link functions (inverse-power, identity, log). To compare the

contributions of the different linear predictors across the different link functions we compare the partial derivatives of the model with regard to the individual predictors. Finally, we test the residuals for remaining trends applying the non-parametric trend analysis.

Code availability. All implementations, input and output data are available upon request and will be made available in a git repository. For damage assessment, we used the natural catastrophe damage framework CLIMADA available at:
https://github.com/CLIMADA-project/climada_python

References

1. Munich Re. NatCatSERVICE Database (Munich Reinsurance Company, Geo Risks Research, Munich). https://www.munichre.com/en/solutions/for-industry-clients/natcatservice.html (2016).
2. Trenberth, K. E. Conceptual framework for changes of extremes of the hydrological cycle with climate change. *Clim. Change* **42**, 327–339 (1999).
3. Ivancic, T. J. & Shaw, S. B. Examining why trends in very heavy precipitation should not be mistaken for trends in very high river discharge. *Clim. Change* **133**, 681–693 (2015).
4. Boer, G. J. Climate change and the regulation of the surface moisture and energy budgets. *Clim. Dyn.* **8**, 225–239 (1993).
5. Allen, M. R. & Ingram, W. J. *Constraints on future changes in climate and the hydrologic cycle*. *Nature* vol. 419 (Nature Publishing Group, 2002).
6. Westra, S., Alexander, L. V. & Zwiers, F. W. Global increasing trends in annual maximum daily precipitation. *J. Clim.* **26**, 3904–3918 (2013).
7. Lehmann, J., Coumou, D. & Frieler, K. Increased record-breaking precipitation events under global warming. *Clim. Change* **132**, 501–515 (2015).
8. Fischer, E. M. & Knutti, R. *Observed heavy precipitation increase confirms theory and early models*. *Nature Climate Change* vol. 6 (Nature Publishing Group, 2016).
9. Do, H. X., Westra, S. & Leonard, M. A global-scale investigation of trends in annual maximum streamflow. *J. Hydrol.* **552**, 28–43 (2017).
10. Najibi, N. & Devineni, N. Recent trends in the frequency and duration of global floods. *Earth Syst. Dyn.* **9**, 757–783 (2018).
11. Berghuijs, W. R., Aalbers, E. E., Larsen, J. R., Trancoso, R. & Woods, R. A. Recent changes in extreme floods across multiple continents. *Environ. Res. Lett.* **12**, 114035 (2017).
12. Jongman, B. *et al.* Declining vulnerability to river floods and the global benefits of

adaptation. *Proc. Natl. Acad. Sci.* **112**, E2271–E2280 (2015).
13. Tanoue, M., Hirabayashi, Y. & Ikeuchi, H. Global-scale river flood vulnerability in the last 50 years. *Sci. Rep.* **6**, 36021 (2016).
14. Huizinga, J., de Moel, H. & Szewczyk, W. *Global flood depth-damage functions : Methodology and the Database with Guidelines*. *Joint Research Centre (JRC)* (2017). doi:10.2760/16510.
15. Formetta, G. & Feyen, L. Empirical evidence of declining global vulnerability to climate-related hazards. *Glob. Environ. Change* **57**, (2019).
16. Barredo, J. I. Normalised flood losses in Europe: 1970–2006. *Nat. Hazards Earth Syst. Sci.* **9**, 97–104 (2009).
17. Bouwer, L. M. Have Disaster Losses Increased Due to Anthropogenic Climate Change? *Bull. Am. Meteorol. Soc.* **92**, 39–46 (2010).
18. Paprotny, D., Sebastian, A., Morales-Nápoles, O. & Jonkman, S. N. Trends in flood losses in Europe over the past 150 years. *Nat. Commun.* **9**, 1–12 (2018).
19. Blöschl, G. *et al.* Changing climate both increases and decreases European river floods. *Nature* **573**, 108–111 (2019).
20. Gudmundsson, L., Leonard, M., Do, H. X., Westra, S. & Seneviratne, S. I. Observed Trends in Global Indicators of Mean and Extreme Streamflow. *Geophys. Res. Lett.* **46**, 756–766 (2019).
21. Mediero, L., Santillán, D., Garrote, L. & Granados, A. Detection and attribution of trends in magnitude, frequency and timing of floods in Spain. *J. Hydrol.* **517**, 1072–1088 (2014).
22. Fantom, N. & Serajuddin, U. The World Bank's classification of countries by income. *World Bank* (2016) doi:10.1596/1813-9450-7528.
23. Guha-Sapir, D. & Below, R. Quality and accuracy of disaster data: A comparative analyse of 3 global data sets. *Work. Pap. Prep. Disaster Manag. Facil. World Bank Bruss.* (2002).
24. Zaherpour, J. *et al.* Worldwide evaluation of mean and extreme runoff from six global-scale hydrological models that account for human impacts. *Environ. Res. Lett.* **13**, 065015 (2018).
25. Beck, H. E. *et al.* Global evaluation of runoff from 10 state-of-the-art hydrological models. *Hydrol. Earth Syst. Sci.* **21**, 2881–2903 (2017).
26. Neumayer, E. & Barthel, F. Normalizing economic loss from natural disasters: A global analysis. *Glob. Environ. Change* **21**, 13–24 (2011).
27. Armal, S., Devineni, N. & Khanbilvardi, R. Trends in Extreme Rainfall Frequency in the Contiguous United States: Attribution to Climate Change and Climate Variability Modes. *J. Clim.* **31**, 369–385 (2018).
28. Witten, I. H., Frank, E., Hall, M. A. & Pal, C. J. *Data Mining: Practical Machine Learning*

Tools and Techniques. *Data Mining: Practical Machine Learning Tools and Techniques* (Elsevier Inc., 2016). doi:10.1016/c2009-0-19715-5.

29. Booth, B. B. B., Dunstone, N. J., Halloran, P. R., Andrews, T. & Bellouin, N. Aerosols implicated as a prime driver of twentieth-century North Atlantic climate variability. *Nature* **484**, 228–232 (2012).
30. Terray, L. Evidence for multiple drivers of North Atlantic multi-decadal climate variability. *Geophys. Res. Lett.* **39**, n/a–n/a (2012).
31. Ting, M., Kushnir, Y. & Li, C. North Atlantic Multidecadal SST Oscillation: External forcing versus internal variability. *J. Mar. Syst.* **133**, 27–38 (2014).
32. Hattermann, F. F. *et al.* Cross-scale intercomparison of climate change impacts simulated by regional and global hydrological models in eleven large river basins. *Clim. Change* **141**, 561–576 (2017).
33. Di Baldassarre, G. *et al. Debates - Perspectives on socio-hydrology: Capturing feedbacks between physical and social processes*. *Water Resources Research* vol. 51 (Blackwell Publishing Ltd, 2015).
34. Cramer, W. *et al.* Detection and attribution of observed impacts. in *Climate Change 2014: Impacts, Adaptation, and Vulnerability. Part A: Global and Sectoral Aspects. Contribution of Working Group II to the Fifth Assessment Report of the Intergovernmental Panel of Climate Change* (eds. Field, C. B. et al.) 979–1037 (Cambridge University Press, 2014).
35. Stone, D. *et al.* The challenge to detect and attribute effects of climate change on human and natural systems. *Clim. Change* **121**, 381–395 (2013).
36. Policelli, F. *et al.* The NASA Global Flood Mapping System. in 47–63 (Springer, Cham, 2017). doi:10.1007/978-3-319-43744-6_3.
37. Mengel, M., Treu, S., Lange, S. & Frieler, K. ATTRICI 1.0 - counterfactual climate for impact attribution. *Submitt. Geosci. Model Dev.* (2020).
38. Sen, P. K. Estimates of the Regression Coefficient Based on Kendall's Tau. *J. Am. Stat. Assoc.* **63**, 1379–1389 (1968).
39. Chandler, R. E. & Scott, E. M. *Statistical Methods for Trend Detection and Analysis in the Environmental Sciences*. *Statistical Methods for Trend Detection and Analysis in the Environmental Sciences* (2011). doi:10.1002/9781119991571.
40. Gosling, S. *et al. ISIMIP2a Simulation Data from Water (global) Sector*. (GFZ Data Services, 2017). doi:10.5880/PIK.2017.010.
41. Pokhrel, Y. *et al.* Incorporating anthropogenic water regulation modules into a land surface model. *J. Hydrometeorol.* **13**, 255–269 (2012).
42. Willner, S. N., Levermann, A., Zhao, F. & Frieler, K. Adaptation required to preserve future high-end river flood risk at present levels. *Sci. Adv.* **4**, eaao1914 (2018).

43. Willner, S. N., Otto, C. & Levermann, A. Global economic response to river floods. *Nat. Clim. Change* **8**, 594–598 (2018).
44. Yamazaki, D., Kanae, S., Kim, H. & Oki, T. A physically based description of floodplain inundation dynamics in a global river routing model. *Water Resour. Res.* **47**, (2011).
45. Zhao, F. *et al.* The critical role of the routing scheme in simulating peak river discharge in global hydrological models. *Environ. Res. Lett.* **12**, 075003 (2017).
46. Hirabayashi, Y. *et al.* Global flood risk under climate change. *Nat. Clim. Change* **3**, 816–821 (2013).
47. Scussolini, P. *et al.* FLOPROS: an evolving global database of flood protection standards. *Nat. Hazards Earth Syst. Sci.* **16**, 1049–1061 (2016).
48. Frieler, K. *et al.* Assessing the impacts of 1.5°C global warming - Simulation protocol of the Inter-Sectoral Impact Model Intercomparison Project (ISIMIP2b). *Geosci. Model Dev.* **10**, 4321–4345 (2017).
49. Murakami, D. & Yamagata, Y. Estimation of gridded population and GDP scenarios with spatially explicit statistical downscaling. *Sustain. Switz.* **11**, 2106 (2019).
50. Klein Goldewijk, K., Beusen, A., Van Drecht, G. & De Vos, M. The HYDE 3.1 spatially explicit database of human-induced global land-use change over the past 12,000 years. *Glob. Ecol. Biogeogr.* **20**, 73–86 (2011).
51. Klein Goldewijk, K., Beusen, A., Doelman, J. & Stehfest, E. Anthropogenic land use estimates for the Holocene - HYDE 3.2. *Earth Syst. Sci. Data* **9**, 927–953 (2017).
52. Geiger, T., Murakami, D., Frieler, K. & Yamagata, Y. Spatially-explicit Gross Cell Product (GCP) time series: past observations (1850-2000) harmonized with future projections according to the Shared Socioeconomic Pathways (2010-2100). *GFZ Data Serv.* (2017).
53. Aznar-Siguan, G. & Bresch, D. N. CLIMADA v1: A global weather and climate risk assessment platform. *Geosci. Model Dev.* **12**, 3085–3097 (2019).
54. Golyandina, N. & Zhigljavsky, A. Singular Spectrum Analysis for Time Series Introductory Paper. 1–3 (2013) doi:10.1007/978-3-642-34913-3.

Acknowledgements. This work was supported by the German Federal Ministry of Education and Research (BMBF) under the research projects SLICE (FKZ: 01LA1829A).

Competing interests. The authors declare no competing interests.

Figures

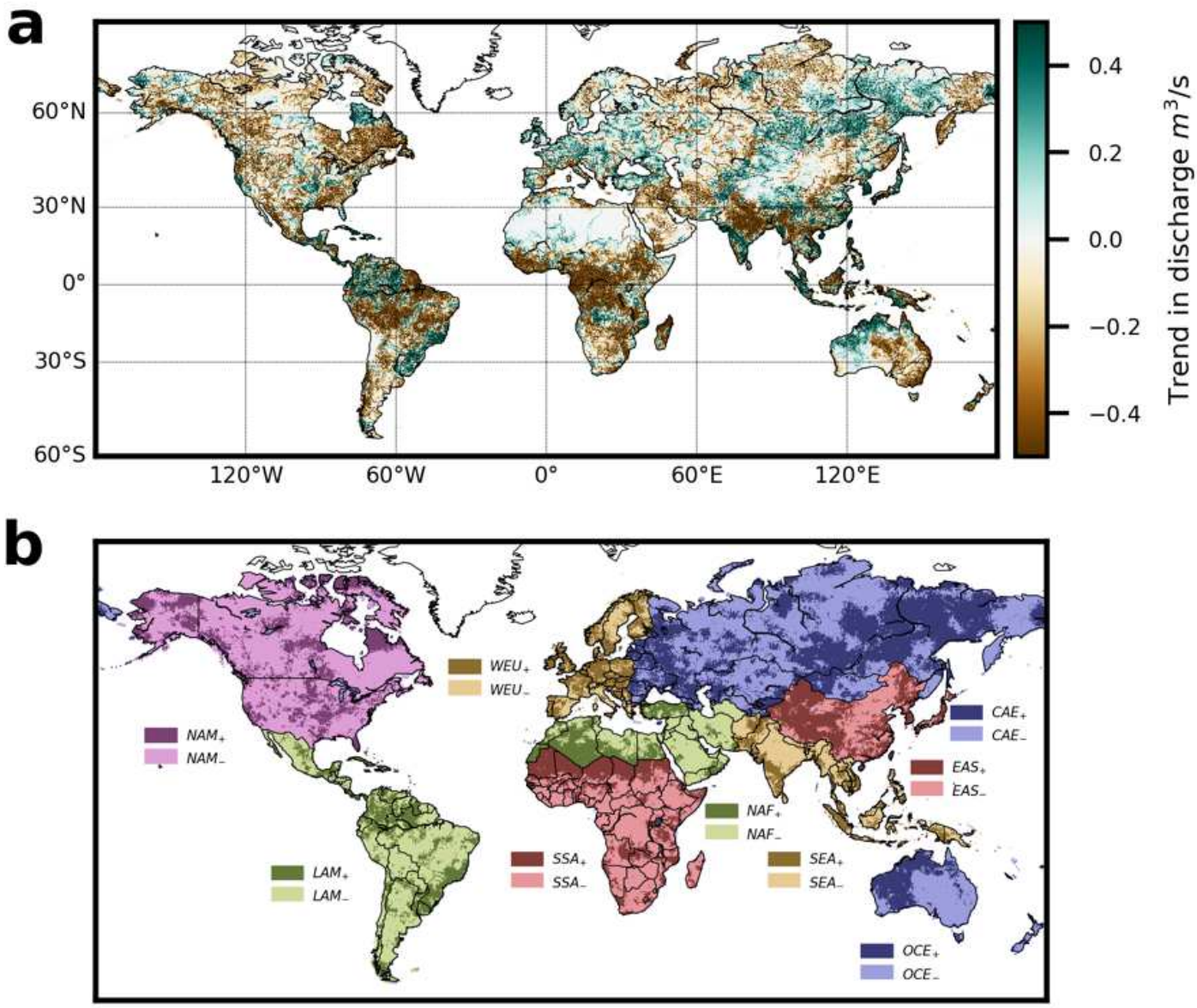

Figure 1

Discharge trends and definition of regions. a Absolute trends in annual maximum discharge in the time period 1971-2010 (significance levels are shown in supplementary Fig. SI3) b Map of the nine geographical world regions: North America (NAM), Eastern Asia (EAS), Western Europe (WEU), Latin America (LAM), Central Asia & Eastern Europe (CAE), South & Sub-Saharan Africa (SSA), South & South-East Asia (SEA), North Africa & Middle East (NAF), Oceania (OCE) chosen according to geographical proximity and similarity of socio-economic structure. These regions are then further divided into subregions with positive (R_+, dark colors) and negative discharge trends (R_-, light colors). Note: The designations employed and the presentation of the material on this map do not imply the expression of

any opinion whatsoever on the part of Research Square concerning the legal status of any country, territory, city or area or of its authorities, or concerning the delimitation of its frontiers or boundaries. This map has been provided by the authors.

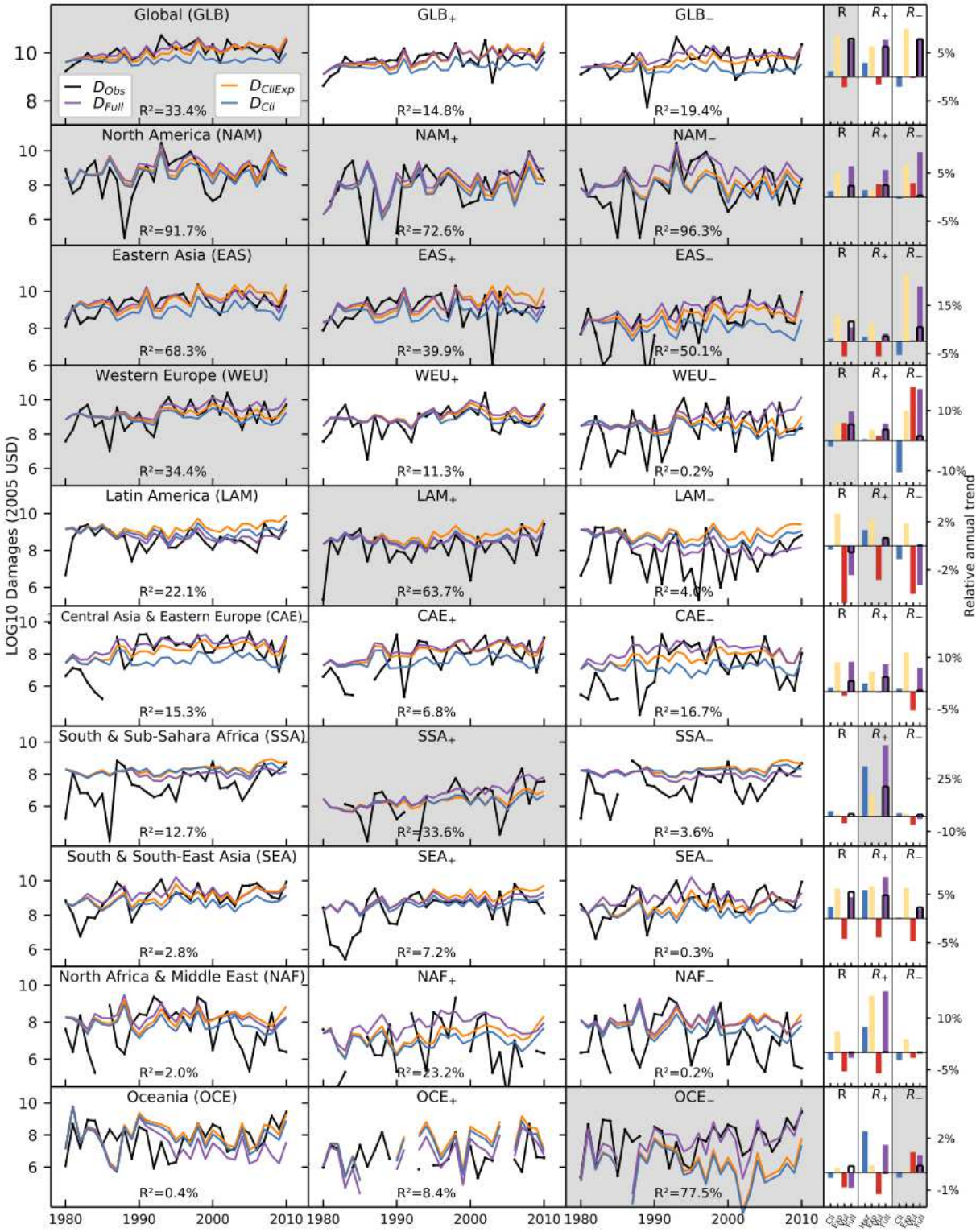

Figure 2

Contributions of changes in climate, exposure, and vulnerability to damages induced by river floods (1980-2010): Time series of observed damages (NatCatService database1 (black) as well as modeled

damages (multi-model median) when accounting for changes in i) climate only (constant 1980 socio-economic conditions, DCli-1980, blue), ii) climate and exposure (DCliExp, orange) keeping vulnerability at 1980 conditions, and iii) in climate, exposure, and vulnerability (DFull, purple) over time for the nine world regions (left main panel), as well as their subregions with homogeneous positive and negative trends in river discharge (middle and right main panels) (cf. Fig. 1). Left Bars in the side panel on the right indicate the relative trend in annual modeled (Full, purple) and observed damages (Full, black squares) and the individual contributions of each driver: climate variability (Cli, blue), exposure (Exp, yellow), vulnerability (Vul, red). R^2 indicates the explained variance of the full model compared to the observed damages. Time series indicating the model-spread are provided in supplementary Fig. SI4.

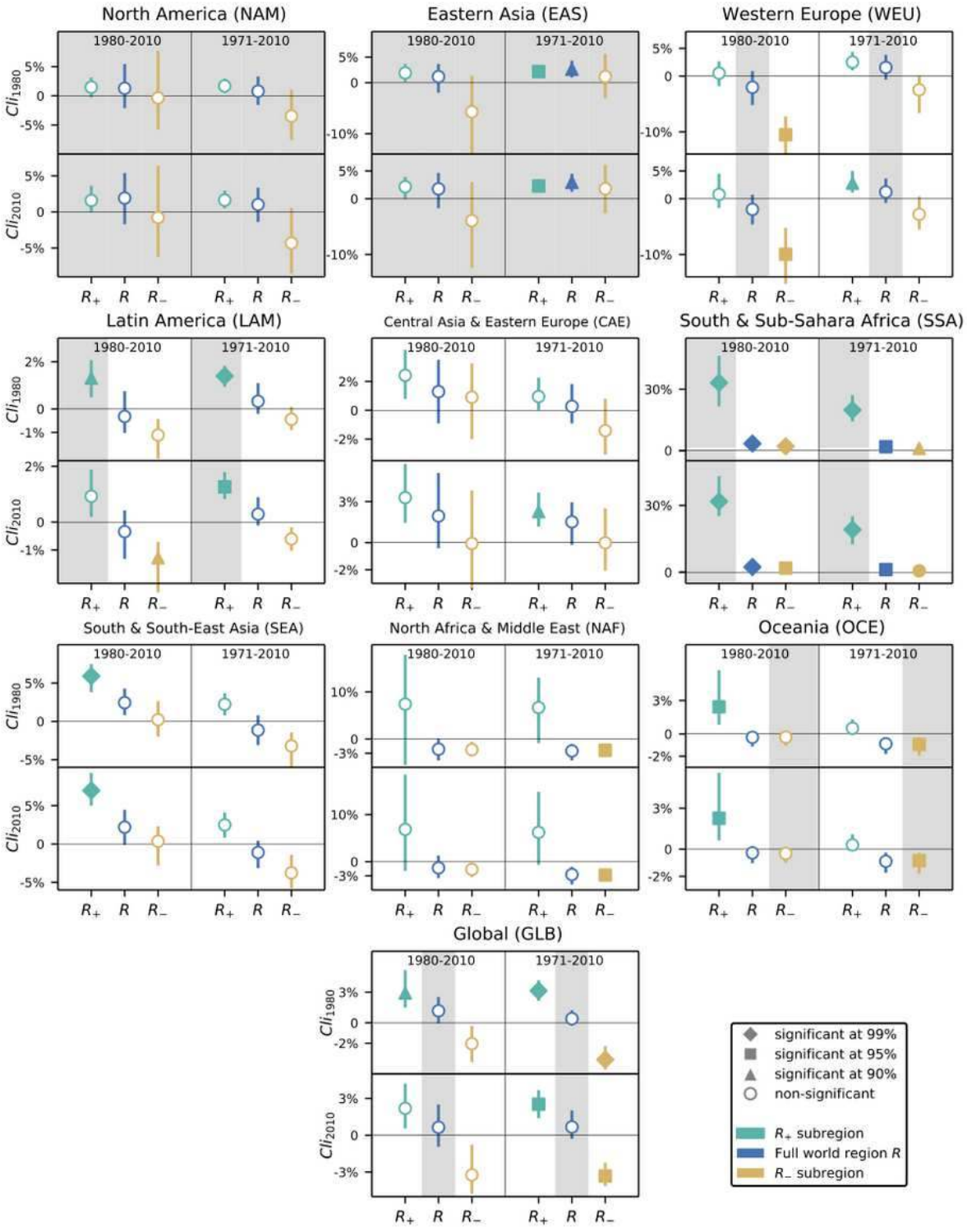

Figure 3

Climate induced trends in economic damages. Shown are trends for each geographical world region (R, blue) as well as in the subregions with positive (R_+, turquoise bars) and negative discharge trends (R_-, brown bars). Uncertainty bars mark the and the quantile of the Theil-Sen-slope estimation. Symbols indicate the statistical significance of the climate trends at various levels. Grey shadings indicate

subregions with high explained variance ($R^2 > 30\%$). Climate-induced trends are calculated for fixed 1980 exposure (□Cli□_(1980)) and fixed 2010 exposure (□Cli□_2010).

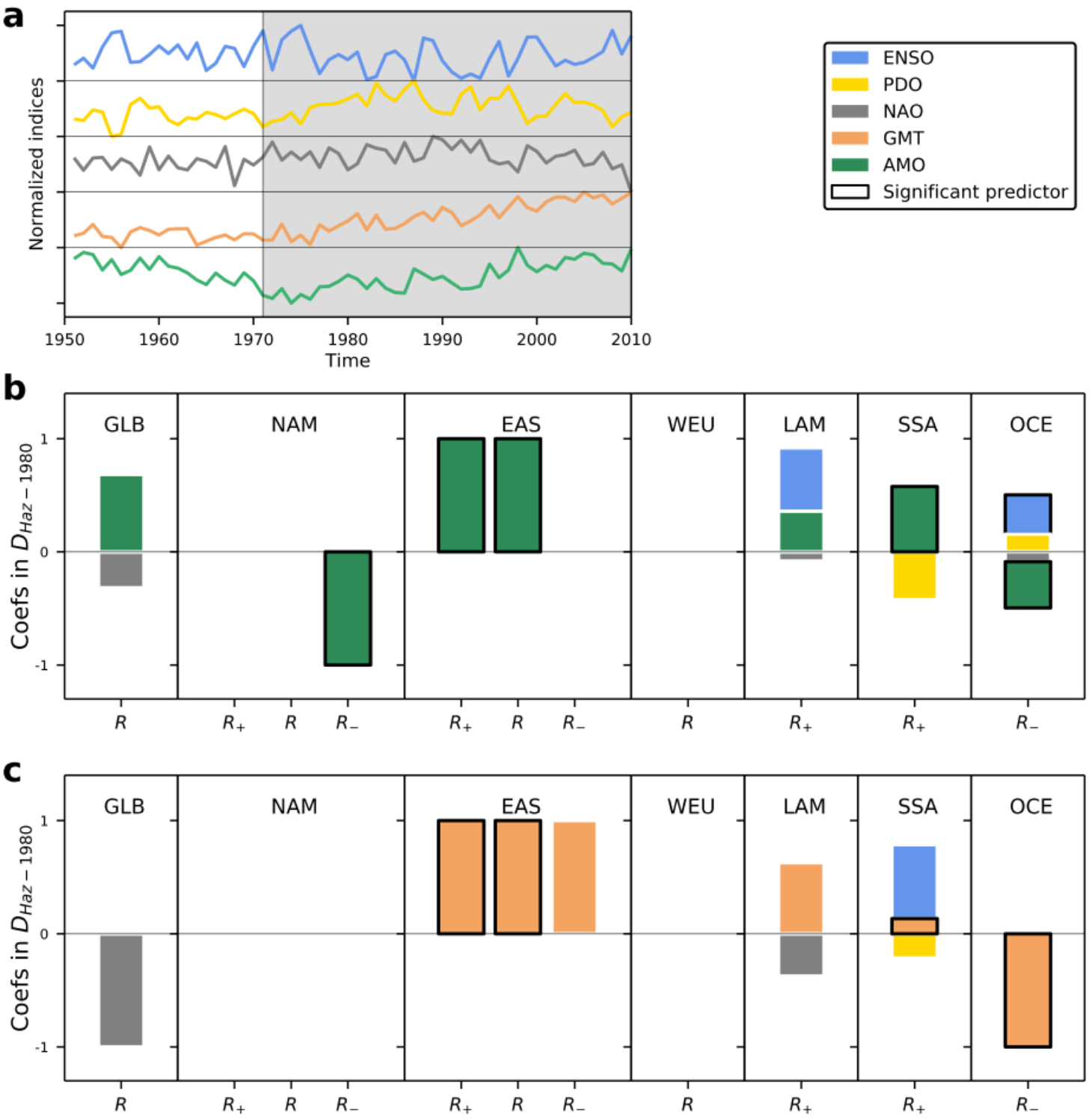

Figure 4

Predictors of climate-induced trends in flood damages. a Normalized indices of ENSO, PDO, NAO, AMO, and GMT from 1971-2010. Only the period 1971-2010 is used for the analysis (gray shading). b Relative shares of the coefficients (Methods) of the linear predictors (ENSO, PDO, NAO, and AMO) included in the

best model (according to the leave-one-out-Cross-Validation) for the damage time series accounting for climate induced trends only (fixed 1980 exposure and vulnerability). Shown are only regions with R2 > 30% for the full model of Fig. 1. Black boxes indicate significant predictors at 90% level. c Same as b, but using ENSO, PDO, NAO, and GMT as predictors.

Supplementary Files

This is a list of supplementary files associated with this preprint. Click to download.

- SupplementaryInformation.pdf